

Chinese NO_x emission reductions and rebound as a result of the COVID-19 crisis quantified through inversion of TROPOMI NO₂ observations

Jieying Ding¹, Ronald J. van der A², Henk Eskes³, Bas Mijling¹, Trissevgeni Stavrou⁴, Jos van Geffen⁵, and Pepijn Veefkind³

¹KNMI Royal Netherlands Meteorological Institute

²KNMI

³Royal Netherlands Meteorological Institute

⁴Royal Belgian Institute for Space Aeronomy

⁵Royal Netherlands Meteorological Institute, De Bilt, Netherlands

November 26, 2022

Abstract

During the COVID-19 lockdown in China low air pollution levels were reported as a consequence of the reduced economic and social activities. Quantification of the pollution reduction is not straightforward due to effects of transport, meteorology, and chemistry. Here we have analysed the NO emission reductions calculated with an inverse algorithm applied to daily NO observations from the TROPOMI instrument onboard the Copernicus Sentinel-5P satellite. This method allows quantification of emission reductions per city, and the analysis of emissions of maritime transport and of the energy sector separately. The reductions we found are 20 to 50% for cities, about 40% for power plants and 15 to 40% for maritime transport depending on the region. The reduction in both emissions and concentrations shows a similar timeline consisting of a sharp reduction around the Spring festival and a slow recovery from mid-February to mid-March.

1
2 **Chinese NO_x emission reductions and rebound as a result of the COVID-19**
3 **crisis quantified through inversion of TROPOMI NO₂ observations**

4
5 **J.Ding¹, R.J. van der A^{1,2}, H.J. Eskes¹, B. Mijling¹, T. Stavrakou³, J.H.G.M. van Geffen¹,**
6 **J.P. Veefkind^{1,4}**

7 ¹ Royal Netherlands Meteorological Institute (KNMI), Utrechtseweg 297, 3731 GA De Bilt, The
8 Netherlands.

9 ² Nanjing University of Information Science & Technology (NUIST), Ningliu Road 219, Nanjing, P.R.
10 China.

11 ³ Royal Belgian Institute for Space Aeronomy (BIRA-IASB), Avenue Circulaire 3, 1180 Brussels,
12 Belgium.

13 ⁴ Delft University of Technology, Stevinweg 1, 2628 CN Delft, The Netherlands

14
15 Corresponding author: Jieying Ding (jieying.ding@knmi.nl)

16 **Key Points:**

- 17 • NO_x emissions derived from TROPOMI observations show reductions for individual
18 Chinese cities of about 35% due to the COVID-19 lockdown.
- 19 • Emissions of coal power plants and maritime transport show strong reductions (25-40%)
20 during the lockdown.
- 21 • Urban emissions rebound in March to levels before the lockdown, while emissions of
22 power plants and maritime transport take longer to recover.

24 **Abstract**

25 During the COVID-19 lockdown in China low air pollution levels were reported as a
26 consequence of the reduced economic and social activities. Quantification of the pollution
27 reduction is not straightforward due to effects of transport, meteorology, and chemistry. Here we
28 have analysed the NO_x emission reductions calculated with an inverse algorithm applied to daily
29 NO₂ observations from the TROPOMI instrument onboard the Copernicus Sentinel-5P satellite.
30 This method allows quantification of emission reductions per city, and the analysis of emissions
31 of maritime transport and of the energy sector separately. The reductions we found are 20 to 50%
32 for cities, about 40% for power plants and 15 to 40% for maritime transport depending on the
33 region. The reduction in both emissions and concentrations shows a similar timeline consisting
34 of a sharp reduction around the Spring festival and a slow recovery from mid-February to mid-
35 March.

36

37 **Plain Language Summary**

38 During the COVID-19 lockdown in China, air quality had strongly improved. Here we study
39 what sources were reduced and how much the reduction per city was. We used TROPOMI
40 observations of the Sentinel-5P satellite, which monitors the Earth's atmosphere daily. We
41 focused on observations of the pollutant 'nitrogen dioxide', an important pre-cursor of air
42 pollution in the atmosphere. With our novel methodology we are able to calculate the pollution
43 back to the sources of the emissions, whether these are big cities, industrial regions, power plants
44 or busy shipping lanes. We applied this method to East China, where the 36 biggest Chinese
45 cities are located. Almost all those cities showed strong emission reductions of 20-50% during
46 the lockdown in February 2020. Besides urban China, we found an average emission reduction
47 of 40% over coal power plants, and a reduction in maritime transport by 15-40% depending on
48 the region. The period of reduced emissions lasted until around the end of February and the
49 emissions slowly returned to normal during the month March 2020. Exception is the region
50 Wuhan, the centre of the COVID-19 crisis, where emissions started to rebound since 8 April, the
51 end of their lockdown period.

52

53 **1 Introduction**

54 The year 2020 is an unprecedented year, with the novel coronavirus, causing the COVID-
55 19 disease spreading over the whole world, infecting millions of people and causing hundreds of
56 thousands of fatalities (WHO, 2020). On 11 March 2020, the World Health Organization (WHO)
57 qualified the spread of COVID-19 as a pandemic. To prevent the spread of the disease, many
58 affected countries implemented COVID-19 regulations such as social distancing, teleworking
59 and the closure of non-essential businesses. China, the first country facing the outbreak of
60 COVID-19, enacted a lockdown from 24 January to 20 March 2020 in the Hubei province where
61 the first cases were reported from its capital Wuhan, while other provinces limited all outdoor
62 activities since the Chinese New Year and gradually resumed the work after 10 February (Tian et
63 al., 2020; Wang et al., 2020).

64 The strict COVID-19 regulations lead to a reduction of road and air traffic, a temporary
65 closing of companies and a decrease of industrial productivity. These in consequence affect
66 emissions of air pollutants, especially from the transport and industry sectors, which are

67 significant sources of NO_x ($\text{NO}_x = \text{NO}_2 + \text{NO}$) in cities. Several studies presented a large decrease
68 of NO_2 concentration during the lockdown period in China from both in-situ and satellite
69 observations (Wang et al., 2020; Huang., 2020). Tropospheric NO_2 column concentrations
70 observed by the TROPOMI (TROPOspheric Monitoring Instrument) on the Sentinel-5P satellite
71 decrease about 35% over China and some areas up to 60% during the COVID-19 regulation
72 period compared to the same period of 2019 (Bauwens et al., 2020; Zhang et al., 2020). In March
73 2020, after the resumption of work and the gradual lifting of the lockdown restrictions, the NO_2
74 concentrations quickly increased to similar levels as in the previous year (Bauwens et al., 2020).
75 Because NO_2 concentrations are affected by meteorology, chemistry and transport, large
76 concentration variations are expected from day to day. Therefore the concentrations alone
77 provide only an indication of the impact of the COVID-19 measures on air pollution. Bottom-up
78 inventories are usually updated with few years delay due to the complexity of gathering all
79 statistic information on source sector, land-use and sector-specific emission factors. A top-down
80 approach using satellite observations has been demonstrated to be able to accurately and quickly
81 provide emission estimates (Stavrakou et al., 2013; Miyazaki et al. 2020). Here we derived the
82 NO_x emissions by using the satellite observations and a chemistry-transport model (CTM). The
83 model is driven by meteorological analyses, accounting for the weather-related variability. The
84 high spatial resolution of the TROPOMI observations and the inverse modelling system allows
85 us to quantify the impact of the COVID-19 measures and distinguish emissions from cities,
86 power plants and maritime transport separately. Recently, NO_x emissions derived from the high
87 resolution NO_2 observations of TROPOMI have been reported by Goldberg et al. (2019) and van
88 der A et al. (2020).

89 To this purpose, we use the DECSO (Daily Emission estimates Constrained by Satellite
90 Observations) algorithm, which has demonstrated its skill to capture emission changes in a short
91 time period at city level (Mijling and van der A, 2012; Ding et al., 2015). This study presents
92 NO_x emissions estimated from Sentinel-5P TROPOMI observations from 2019 to April 2020
93 over East Asia. The high spatial resolution satellite observations and daily global coverage allow
94 us to monitor fast emission changes per city due to the implementation and to the relaxing of
95 COVID-19 regulations.

96

97 **2 Methodology**

98

99 **2.1 NO_2 observations by TROPOMI**

100 The Copernicus Sentinel-5P satellite carries the TROPOMI instrument (Veeffkind et al,
101 2012). TROPOMI is a spectrometer combining a high spectral resolution with high spatial
102 resolution ($3.5 \times 5.5 \text{ km}^2$ at nadir for the NO_2 observations), high signal-to-noise ratios and a
103 daily global coverage. Despite the much smaller footprints, the spectral fits of the individual
104 TROPOMI ground pixels have 30% smaller noise than those from the Ozone Monitoring
105 Instrument (OMI) and the average values agree well to within 5% (van Geffen et al, 2020).

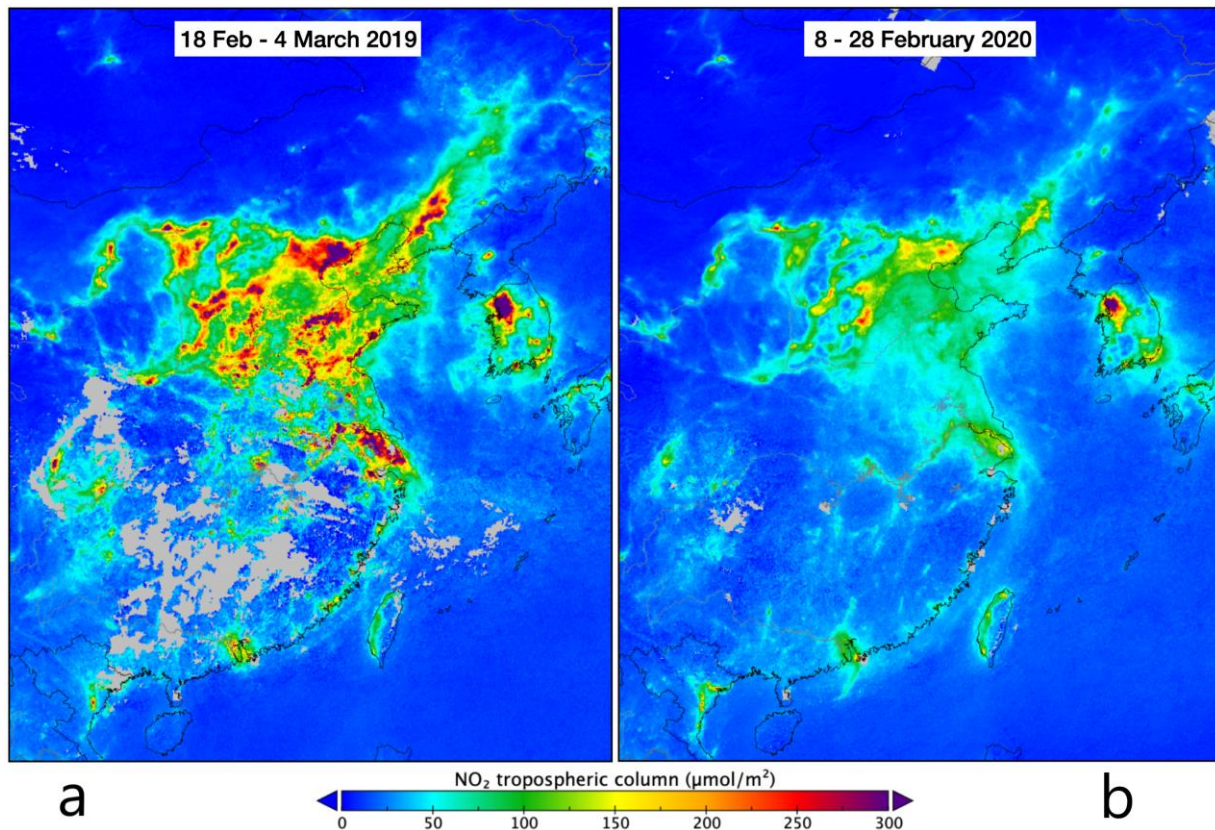
106 A major difference in the retrieval of the tropospheric vertical column compared to OMI
107 is the retrieval of the effective cloud pressure, derived from the $\text{O}_2\text{-A}$ band in the near infrared
108 with the FRESCO algorithm for TROPOMI, and from the $\text{O}_2\text{-O}_2$ absorption band in OMI. The
109 currently available TROPOMI product (versions 1.2 and 1.3) has tropospheric column which are

110 about 20% lower than OMI over Eastern China, and this is largely attributed to the cloud
111 pressure retrieval difference (van Geffen et al., 2019). In the relative comparisons discussed in
112 this paper (e.g. 2020 versus 2019) we expect a large part of such a multiplicative bias to cancel
113 out.

114 The TROPOMI tropospheric NO₂ columns are pre-processed into “super-observations”,
115 representing the integrated average of the TROPOMI observations over the 0.25° x 0.25° grid
116 cells of the model after filtering for clouds. A super-observation may contain up to 25 individual
117 observations of TROPOMI. The super-observation error takes into account spatial correlations
118 between individual TROPOMI observations as well as representativity errors in the case of
119 incomplete coverage. Averaging kernels are also computed for these super-observations, and are
120 used in the emission estimates described below. This has the advantage that the assimilation
121 result becomes independent of the coarser-resolution of the a priori profile used in the retrieval
122 of the tropospheric column.

123 Figure 1 shows the mean TROPOMI NO₂ tropospheric column observations gridded on a
124 0.02° by 0.02° grid for the periods 8-28 February 2020 compared with 18 February to 4 March
125 2019, both after the Chinese New Year holidays. Very prominent concentration reductions are
126 observed in February 2020 compared to 2019.

127



128

129

130 **Figure 1.** TROPOMI NO₂ columns over East China after the Chinese New Year in 2019 (a) and
131 2020 (b).

132

133

134 2.2 NO_x emissions from DECSO

135 DECSO is a state-of-the-art inverse algorithm developed by Mijling and van der A
136 (2012) to update daily emissions of short-lived atmospheric constituents using an extended
137 Kalman filter, in which emissions are translated to concentrations via a CTM and compared to
138 the satellite observations. The sensitivity of concentrations to emissions is calculated from a
139 trajectory analysis to account for transport of the short-lived gas by using a single CTM forward
140 run. DECSO has been successfully applied to NO₂ observations from OMI and TROPOMI over
141 different regions (www.globemission.eu). In this study, daily NO_x emissions from 2019 to April
142 2020 over East Asia (102–120°E, 18–50°N) are derived with DECSO by using the Eulerian
143 regional off-line CTM CHIMERE v2013 (Menut et al., 2013) and TROPOMI NO₂ observations.
144 The implementation of CHIMERE v2013 in DECSO is described in Ding et al. (2015). The
145 latest development and validation of DECSO are presented in previous studies (Ding et al., 2017;
146 van der A et al., 2020). The novelty in our current approach is that we applied DECSO to the
147 super-observations of TROPOMI instead of directly using individual TROPOMI observations.

148

149 2.3 In-situ observations

150 More than 1500 in-situ stations covering all major cities in China are operated by the
151 China National Environmental Monitoring Center. They provide hourly observations of the
152 pollutants PM₁₀, PM_{2.5}, O₃, NO₂, SO₂, and CO (Bai et al., 2020). NO₂ is measured by a
153 chemiluminescence technique (Zhang & Zhao, 2015). Data can be accessed via web-sites of
154 third parties, such as www.pm25.in and www.aqicn.org. For this study we have averaged the
155 various in-situ NO₂ observations in a city to a single value per hour for each of 36 selected major
156 cities. For comparison with model results, we calculated a daily value based on the observations
157 from 10:00 to 18:00 local time. The daytime selection is due to large inaccuracies in simulations
158 of the nighttime boundary layer height.

159

160 2.4 Ensemble modelling

161 An operational multi-model forecasting system for air quality has been developed to
162 provide air quality services for urban areas of China (Brasseur et al., 2019, Petersen et al., 2019).
163 This system has been conceived and developed in the framework of two EU-funded FP-7
164 projects: MarcoPolo and PANDA. The ensemble model system includes nine global and regional
165 chemistry-transport models from different research institutes from Europe and China. The
166 ensemble service has a typical resolution of about 20 km. It provides daily forecasts of ozone,
167 nitrogen oxides, and particulate matter for the 36 largest urban areas of East China (i.e.
168 population higher than 3 million according to the census of 2010). These individual 3-day
169 forecasts as well as the mean and median concentrations are publicly accessible
170 (<http://www.marcopolo-panda.eu>). The emission inventories used as input to the models of the

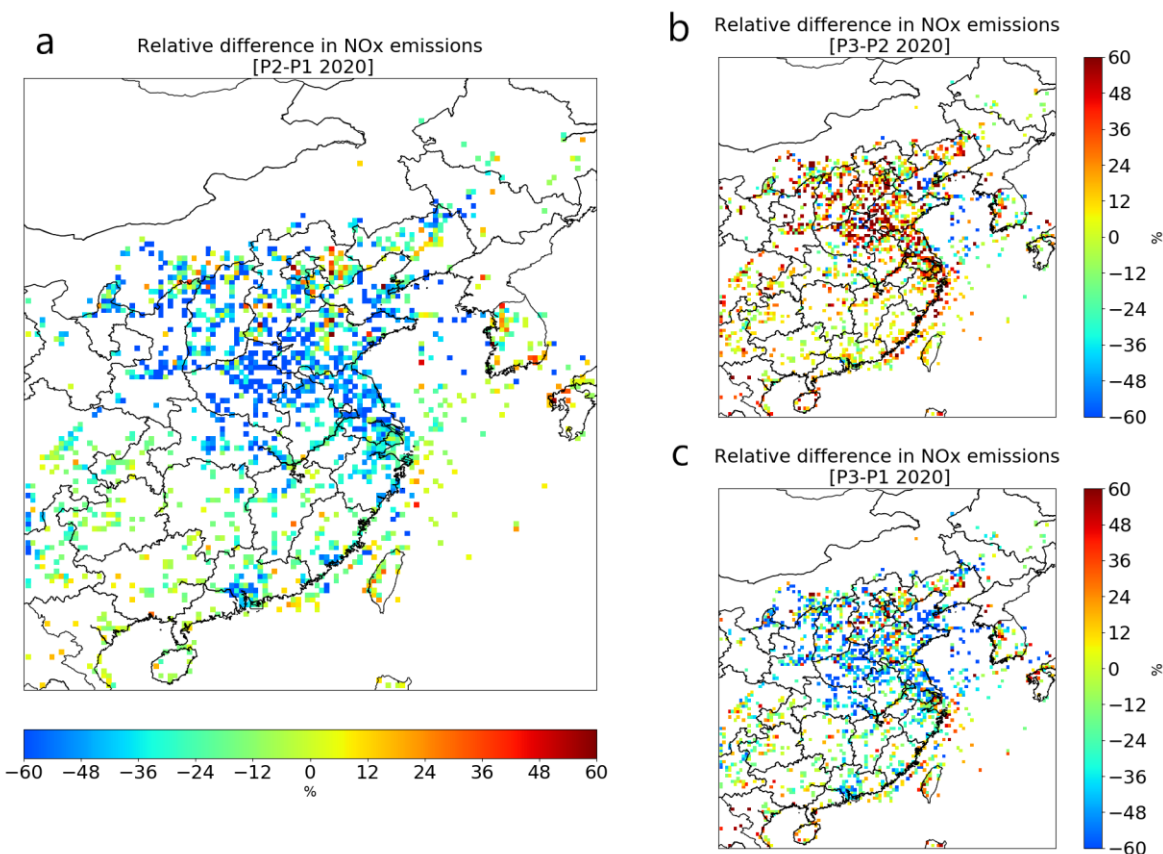
171 ensemble do not account for the Chinese New Year or the COVID-19 lock down period.
172 Therefore, the ensemble model represents the business-as-usual scenario.

173

174 **3 NO_x emissions reductions**

175 NO_x emissions have been affected since the strict regulations started in China, especially
176 in the Hubei Province. We select three periods to quantify the impact of the COVID-19
177 regulations. The first period (P1) is three weeks before the implementation of the COVID-19
178 regulations, 3 to 23 January in 2020, which is also just before the Chinese New Year. The second
179 period (P2) is 8 to 28 February, which is regarded as the regulation period. The third period (P3)
180 is from 18 March to 7 April, when most regions in China resumed working. Figure 2 shows the
181 relative changes of emissions during the selected 3 periods over the grid cells with high
182 anthropogenic (above 3kg N/km²/day) NO_x emissions. We observe a strong decrease of NO_x
183 emissions over China in P2 compared to P1 (Figure S1 shows the emission changes on
184 provincial level). A few grid cells with increased emissions often coincide with industrial areas.
185 In P3, NO_x emissions increased compared to P2 but are still lower than in P1 because of the step-
186 wise resumption of work and social life. The NO_x emissions in South Korea are not significantly
187 changed in P2 compared to the changes in China during the three periods (Figure S1), because
188 South Korea adopted less restrictive COVID-19 regulations, mostly on voluntary basis (Bauwens
189 et al., 2020). The emissions due to sea-transport from Shanghai to Guangzhou are less affected
190 than the transport over land and are found to decrease by about 25% in P2 and increase again
191 with 18% in P3 in comparison to P2. A more significant emission decline was found in the
192 Yellow Sea and Bohai area, where NO_x emissions reduced by about 41% in P2 and continued
193 decreasing by 6% in P3.

194



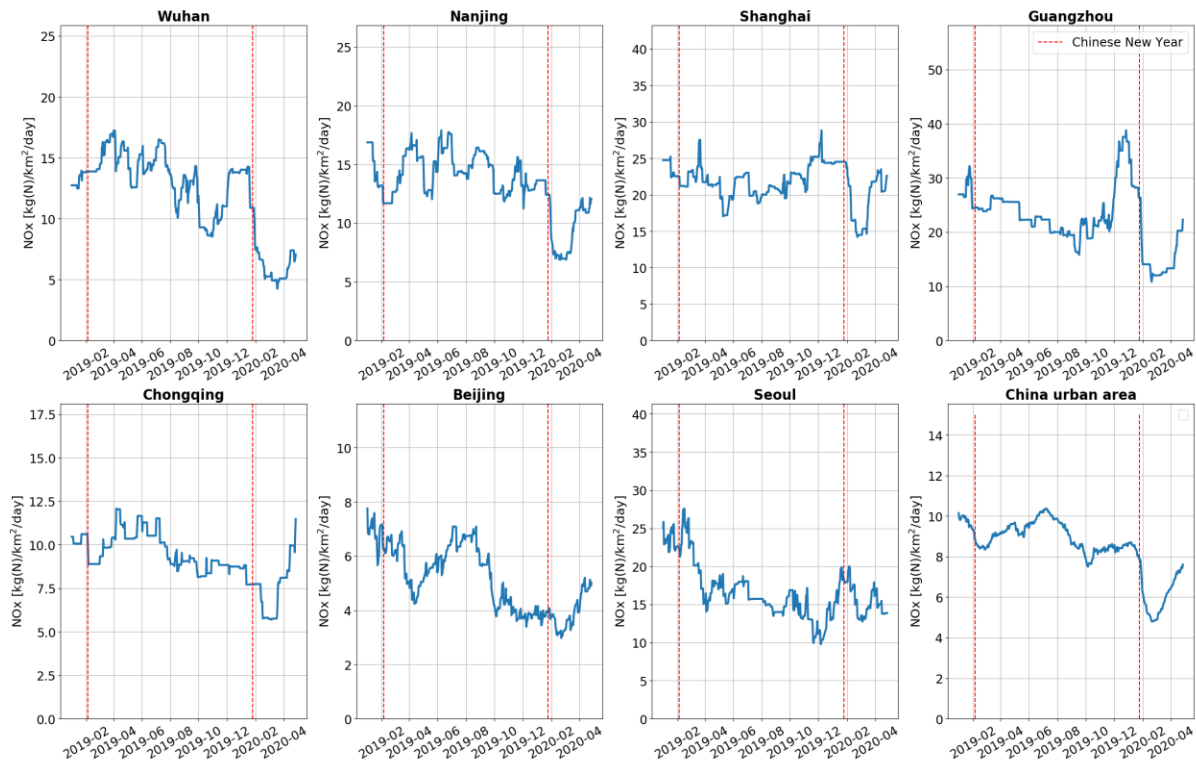
195

196 **Figure 2.** The relative difference in NO_x emissions between (a) P2 and P1; (b) P3 and P2 (c) P3
 197 and P1. P1 is 3-23 January. P2 is 8-28 February. P3 is 18 March to 7 April. The changes in
 198 emissions are shown in the figure for emissions higher than 3 kg(N)/km²/day in P1.

199

200 At city level changes in NO_x emissions started from January 2019. Figure 3 shows the
 201 time series of emissions at 6 large cities in China and in Seoul, the capital of South Korea. We
 202 infer a very strong NO_x emission decrease of more than 50% during and after the 2020 Chinese
 203 New Year in Wuhan, where the COVID-19 outbreak was first recorded and very strict lockdown
 204 regulations were adopted, while an almost negligible reduction in NO_x emissions is derived
 205 during the 2019 Chinese New Year. At the other five Chinese cities, we also observe a much
 206 stronger decrease after the Chinese New Year in 2020 than in 2019. In addition, the duration of
 207 the period with low emissions is much longer. Most cities in China display a stronger decrease in
 208 2020 (see Table S1), which is attributed to the COVID-19 measures. The averaged NO_x
 209 emission reduction at the selected cities shown in table S1 is 35%. We also calculate the average
 210 reduction of grid cells containing urban areas selected by using the land-use data of the
 211 GlobCover Land Cover dataset. The inferred emission reduction is about 35% in urban areas,
 212 which is the same as the average reduction in the selected cities. Note that the NO_x emissions
 213 are usually lower by about 10% during the Chinese New Year with less business and industrial
 214 activities (Ding et al., 2017). The time line of NO_x emissions in Beijing show a slightly different
 215 pattern with a relatively low reduction during the COVID-19 lockdown, but already strong
 216 emission reductions during the politically important “two-sessions” meeting in March 2019 and

217 especially the celebration of 70th national anniversary of China around 1 October 2019, when
 218 many factories were closed and strict emission regulations were enforced (Yang et al., 2020).
 219 Figure 3 also shows that the NO_x emissions start to increase again in March, in line with the step-
 220 by-step recovery of the human activities. Except for Wuhan with the emission rebound after 8
 221 April, when the lockdown was lifted, by the end of March all cities reached a level of NO_x
 222 emissions close to what was observed in the same period in 2019. This is consistent with the
 223 economic target of China. It has been reported that China has a temporary economic setback due
 224 to the COVID-19 outbreak, but will accelerate the return to the pre-crisis economic level (e.g.
 225 Ouyang, 2020).



226
 227 **Figure 3.** Time series (1 January 2019 to 28 April 2020) of daily NO_x emissions in 7 cities and
 228 urban China. The red dashed lines indicate the Chinese New Year in 2019 and 2020. 6 Chinese
 229 cities are considered (Wuhan, Nanjing, Shanghai, Guangzhou, Chongqing and Beijing) as well as
 230 Seoul.

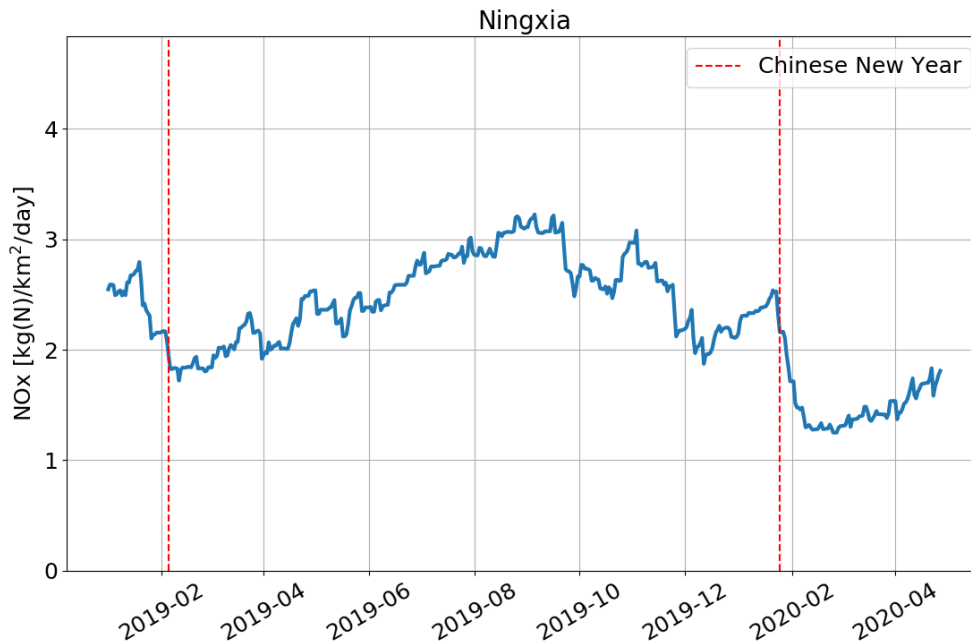
231

232

233 Besides the urban emissions, we find strong reductions of NO_x emissions from coal
 234 power plants. Figure 4 shows time series of NO_x emissions from the Ningxia Province, where the
 235 main sources of NO_x are fossil fuel power plants (van der A et al., 2017). Ningxia province can
 236 serve as an indication of the national energy production by coal power plants. It has a population
 237 of about 6 millions, only 0.4% of the total population of China. Its coal production and electricity
 238 generation from coal power plants are in the top ten list of provinces and about 80% of the
 239 generated energy is consumed by the industry (Ningxia Statistics Bureau, 2019). Our inversion
 240 results indicate that after the 2020 Chinese New Year, NO_x emissions dropped about 40% in this

241 province, 20% more than in 2019 New Year period. This shows the impact of the COVID-19
 242 regulations on the energy production, especially in the industrial sector. According to the
 243 National Bureau of Statistics of China (2020), the total profit of the first three months in 2020
 244 made by industrial enterprises decreased around 40% in China compared to the same period of
 245 the previous year. The shrinking of the industrial economy results in lower energy consumption,
 246 which is clearly reflected by the decrease of NO_x emissions from power plants.

247



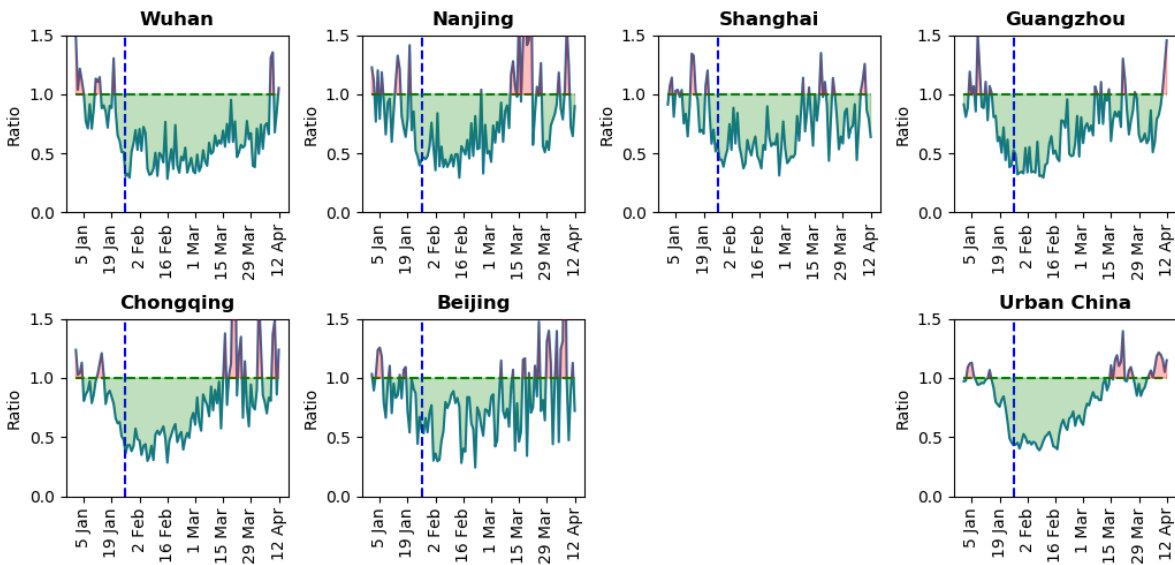
248 **Figure 4.** Time series (1 January 2019 to 28 April 2020) of daily NO_x emissions in Ningxia
 249 Province. The red dashed lines indicate the Chinese New Year in 2019 and 2020.
 250

251

252 4 Concentration reductions

253 Although the NO₂ concentrations at the surface are affected by transport, meteorology
 254 and chemical lifetime, more or less similar reductions are to be expected for the total column. To
 255 eliminate the effect of meteorology and transport we compare the measurements of in-situ
 256 stations with the MarcoPolo-Panda ensemble model driven by emission inventories (business-as-
 257 usual model), which are not corrected for the effects of either Spring Festival or the COVID-19
 258 crisis. A possible bias between measurements and model is corrected for by normalizing the
 259 results for the first two weeks of January. In Figure 5 the ratio between in-situ measured NO₂ and
 260 the modelled NO₂ is shown. The concentration reductions are shown as green area, while
 261 increased concentrations are shown in red. The reduction starts around the Chinese New Year
 262 and ends in March. Exception is the concentration level of Wuhan that becomes similar to that of
 263 the business-as-usual scenario after the first week of April. Table S1 shows the concentration
 264 reduction in P2 compared to P1 for the selected 36 cities. The average concentration reduction is
 265 41%, while for emissions the reduction is 35%. A striking difference between Wuhan and the
 266 other Chinese cities is the longer duration (by about one month) of the concentration reductions.

267



268

269 **Figure 5.** Measured NO₂ concentrations (from 1 January to 12 April 2020) compared to
 270 concentrations of the business-as-usual scenario. Cities are chosen similar to Figure 3, except for
 271 Seoul. The Chinese New Year is indicated by the blue dashed line.

272

273 5 Conclusions

274 To study the impact of the COVID-19 regulations on NO_x emissions (one of the key
 275 ingredients determining air pollution), we derived daily NO_x emissions at a resolution of 0.25° ×
 276 0.25° over East Asia from 2019 to March 2020 by applying the inverse algorithm DECSO to
 277 observations from TROPOMI. By grouping the emission into three periods of before, during and
 278 after the COVID-19 regulations, we quantified the emission changes on the small spatial scale of
 279 city level and from different emission sources such as sea-transport and the energy sector. The
 280 observations suggest emission reductions of 20% to 50% for cities. The emissions reduction of
 281 40% in the Ningxia province reflects the impact of the lockdown measures on the energy sector.
 282 Maritime transport is also affected during the COVID-19 regulations, although its emissions
 283 reductions are dependent on the region. Along the ship track from Shanghai to Guangzhou, the
 284 NO_x emissions decreased by 25% during the lockdown and increased again by 18% after the
 285 work resumption. While in the region of the Yellow sea and Bohai sea, the emissions decrease
 286 by 40% and continued decreasing with another 6% also in March. To further analyze the impact
 287 of emission reductions, we compared the in situ NO₂ concentration measurements with simulated
 288 surface concentrations from models using unaltered emissions. The emission reductions follow a
 289 similar timeline as the surface NO₂ concentrations, which show a sharp reduction around the
 290 Chinese New Year and a slow recovery from mid-February to mid-March. Wuhan, the city of the
 291 epicenter of the COVID-19 crisis, shows large emission reductions in both February and March,
 292 reaching nominal levels in April. In general, we found that activities in the cities returned to
 293 normal in March, while as an indicator of the economy, emissions of energy production and
 294 international maritime transport, took a longer time to return to pre-COVID-19 levels (Table S2).

295 With the NO_x emissions derived from DECSO using observations from TROPOMI, we
 296 are able to get detailed information about the impact on emission changes due to the COVID-19

297 regulations by accounting for the influence of meteorology, lifetime and transport of the air
298 pollutants. As the COVID-19 crisis progressively affects all continents, the public health
299 regulations implemented by various countries may have different contributions to air quality.
300 Applying our methodology to different regions can help to quantify the impact of the NO_x
301 emission reductions by the different regulations on not only the improvement of air quality from
302 urban to local to regional scale.

303 **Acknowledgments, Samples, and Data**

304 This research has been supported by the project “Impact study of COVID-19 lockdown
305 measures on air quality and climate” (2020) of the European Space Agency. This publication
306 contains modified Copernicus Sentinel-5P data 2019-2020. TROPOMI data version 1.2.2 and
307 1.3.0 used is available at <https://s5phub.copernicus.eu/>. We acknowledge the ESA GlobCover
308 2009 project for the land use data set on http://due.esrin.esa.int/page_globcover.php. The NO_x
309 emissions dataset in this study is available on www.globemission.eu.

311 **References**

312 Bai, K., Li, K, Guo, J., Yang, Y., Chang, N.-B. (2020). Filling the gaps of in situ hourly PM_{2.5}
313 concentration data with the aid of empirical orthogonal function analysis constrained by diurnal
314 cycles. *Atmospheric Measurement Techniques*, 13, 3, 1213-1226, DOI: 10.5194/amt-13-1213-
315 2020.

316
317 Bauwens, M., Compernelle, S., Stavrou, T., Müller, J.-F., van Gent, J., Eskes, H., et al. (2020).
318 Impact of coronavirus outbreak on NO₂ pollution assessed using TROPOMI and OMI
319 observations. *Geophysical Research Letters*, <https://doi.org/10.1029/2020GL087978>, 2020

320
321 Brasseur, G. P., Xie, Y., Petersen, A. K., Bouarar, I., Flemming, J., Gauss, M., et al. (2019).
322 Ensemble forecasts of air quality in eastern China - Part 1: Model description and
323 implementation of the MarcoPolo-Panda prediction system, version 1, *Geosci. Model Dev.*, 12,
324 33-67, <https://doi.org/10.5194/gmd-12-33-2019>.

325
326 Ding, J., van der A, R. J., Mijling, B., Levelt, P. F., & Hao, N. (2015). NO_x emission estimates
327 during the 2014 Youth Olympic Games in Nanjing. *Atmos. Chem. Phys.*, 15(16), 9399-9412.
328 doi:10.5194/acp-15-9399-2015

329
330 Ding, J., Miyazaki, K., van der A, R. J., Mijling, B., Kurokawa, J. I., et al. (2017).
331 Intercomparison of NO_x emission inventories over East Asia. *Atmos. Chem. Phys.*, 17(16),
332 10125-10141. doi:10.5194/acp-17-10125-2017

333
334 Goldberg, D., L., Lu, Z., Streets, D., G., de Foy, B., Griffin, D., McLinden, C., A., et al. (2019).
335 Enhanced Capabilities of TROPOMI NO₂: Estimating NO_x from North American Cities and

336 Power Plants, *Environ. Sci. Technol.*, 53, 21, 12594-12601,
337 <https://doi.org/10.1021/acs.est.9b04488>.

338

339 Gu, J., Chen, L., Yu, C., Li, S., Tao, J., Fan, M., et al. (2017) Ground-Level NO₂ Concentrations
340 over China Inferred from the Satellite OMI and CMAQ Model Simulations. *Remote Sens.*, 9(6),
341 519, <https://doi.org/10.3390/rs9060519>

342

343 Huang, X., Ding, A., Gao, J., Zheng, B., Zhou, D., et al. (2020). Enhanced secondary pollution
344 offset reduction of primary emissions during COVID-19 lockdown in China. *EarthArXiv.*, April
345 13. <https://doi.org/10.31223/osf.io/hvuzy>

346

347 Menut, L., Bessagnet, B., Khvorostyanov, D., Beekmann, M., Blond, N., Colette, A., et al.
348 (2013). CHIMERE 2013: A model for regional atmospheric composition modelling.
349 *Geoscientific Model Development*, 6(4), 981–1028. <https://doi.org/10.5194/gmd-6-981-2013>

350

351 Mijling, B., and van der A, R. J. (2012). Using daily satellite observations to estimate emissions
352 of short-lived air pollutants on a mesoscopic scale. *Journal of Geophysical Research:*
353 *Atmospheres*, 117(D17). doi:10.1029/2012JD017817

354

355 Miyazaki, K., Bowman, K., Sekiya, T., Eskes, H., Boersma, F., Worden, H., et al. (2020). An
356 updated tropospheric chemistry reanalysis and emission estimates, TCR-2, for 2005–2018, *Earth*
357 *Syst. Sci. Data Discuss.*, <https://doi.org/10.5194/essd-2020-30>, in review.

358

359 National Bureau of Statistics of China (2020). Available online:
360 http://www.stats.gov.cn/english/PressRelease/202004/t20200428_1742015.html (last access
361 date: 3 May 2020)

362

363 Ningxia Statistics Bureau (2019). The Achievements of Economic and Social Development
364 during the last 70 years, part 3, in Chinese. Available online:
365 http://tj.nx.gov.cn/tjxx/201909/t20190923_1750612.html (last access date: 9 May 2020)

366

367 Ouyang S. (2020). COVID-19 will not alter China's growth story, top economic regulator says,
368 *China Daily*. Available online:
369 <https://global.chinadaily.com.cn/a/202004/20/WS5e9d51f8a3105d50a3d1779c.html> (last access
370 date: 27 April 2020)

371

372 Petersen, A. K., Brasseur, G. P., Bouarar, I., Flemming, J., Gauss, M., Jiang, F., et al (2019).
373 Ensemble forecasts of air quality in eastern China - Part 2: Evaluation of the MarcoPolo-Panda

374 prediction system, version 1. *Geosci. Model Dev.* 12, 1241-1266, <https://doi.org/10.5194/gmd->
375 12-1241-2019.

376

377 Shindell, D. T., Faluvegi, G., Koch, D. M., Schmidt, G. A., Unger, N., & Bauer, S. E. (2009).
378 Improved Attribution of Climate Forcing to Emissions. *Science*. 326(5953), 716-718.
379 doi:10.1126/science.1174760

380

381 Stavrakou, T., Müller, J.-F., Boersma, K. F., van der A, R. J., Kurokawa, J., Ohara, T., and
382 Zhang, Q. (2013). Key chemical NO_x sink uncertainties and how they influence top-down
383 emissions of nitrogen oxides, *Atmos. Chem. Phys.*, 13, 9057–9082, <https://doi.org/10.5194/acp->
384 13-9057-2013,.

385

386 Tian, H., Liu, Y., Li, Y., Wu, C.-H., Chen, B., Kraemer, M. U. G., et al. (2020). An investigation
387 of transmission control measures during the first 50 days of the COVID-19 epidemic in China.
388 *Science*, eabb6105. doi:10.1126/science.abb6105

389

390 van der A, R. J., Mijling, B., Ding, J., Koukouli, M. E., Liu, F., Li, Q., et al. (2017). Cleaning up
391 the air: effectiveness of air quality policy for SO₂ and NO_x emissions in China. *Atmos. Chem.*
392 *Phys.*, 17(3), 1775-1789. doi:10.5194/acp-17-1775-2017

393

394 van der A, R. J., de Laat, A. T. J., Ding, J., & Eskes, H. J. (2020). Connecting the dots: NO_x
395 emissions along a West Siberian natural gas pipeline. *npj Climate and Atmospheric Science*,
396 3(1), 16. doi:10.1038/s41612-020-0119-z

397

398 van Geffen, J., Boersma, K. F., Eskes, H., Sneep, M., ter Linden, M., Zara, M., and Veefkind, J.
399 P.: S5P TROPOMI NO₂ slant column retrieval: method, stability, uncertainties and comparisons
400 with OMI, *Atmos. Meas. Tech.*, 13, 1315–1335, <https://doi.org/10.5194/amt-> 13-1315-2020,
401 2020.

402

403 van Geffen, J. H. G. M., Eskes, H. J., Boersma, K. F., Maasackers, J. D., and Veefkind, J. P.
404 (2019). TROPOMI ATBD of the total and tropospheric NO₂ data products, Report S5P-KNMI-
405 L2-0005-RP, version 1.4.0, released 6 February 2019, KNMI, De Bilt, the Netherlands, available
406 at: <http://www.tropomi.eu/documents/atbd/>, last access: 17 March 2020.

407

408 Veefkind, J. P., Aben, I., McMullan, K., Förster, H., de Vries, J., Otter, G., et. al. (2012).
409 TROPOMI on the ESA Sentinel-5 Precursor: A GMES mission for global observations of the
410 atmospheric composition for climate, air quality and ozone layer applications. *Remote Sensing of*
411 *Environment*, 120, 70-83. doi:<https://doi.org/10.1016/j.rse.2011.09.027>

412

413

414 Wang, P., Chen, K., Zhu, S., Wang, P., & Zhang, H. (2020). Severe air pollution events not
415 avoided by reduced anthropogenic activities during COVID-19 outbreak. *Resources,*
416 *Conservation and Recycling*, 158, 104814. doi:<https://doi.org/10.1016/j.resconrec.2020.104814>

417

418 WHO (2020). The World Health Organization. Coronavirus Disease (COVID-19) Pandemic.
419 Available online: <https://www.who.int/emergencies/diseases/novel-coronavirus-2019> (last access
420 date: 27 April 2020)

421

422 Yang, Y., Wang, Y., Yao, D., Zhao, S., Yang, S., et al. (2020). Significant decreases in the
423 volatile organic compound concentration, atmospheric oxidation capacity and photochemical
424 reactivity during the National Day holiday over a suburban site in the North China Plain,
425 *Environmental Pollution*, Volume 263, Part A, 114657,
426 <https://doi.org/10.1016/j.envpol.2020.114657>.

427

428 Zhang, R., Zhang, Y., Lin, H., Feng, X., Fu, T.-M., & Wang, Y. (2020). NO_x Emission
429 Reduction and Recovery during COVID-19 in East China. *Atmosphere*, 11(4), 433

430

431 Zhang, Y., Cao, F. (2015) Fine particulate matter (PM_{2.5}) in China at a city level. *Sci Rep* 5,
432 14884. <https://doi.org/10.1038/srep14884>

433

434

435

436

437